Original Paper

phys. stat. sol. (b) **244**, No. 6, 2127–2137 (2007) / **DOI** 10.1002/pssb.200642370

Compositional dependence of optical and vibrational properties of strontium barium niobate ($Sr_xBa_{1-x}Nb_2O_6$)

C. David, A. Tunyagi, K. Betzler, and **M. Wöhlecke***

Fachbereich Physik, Universität Osnabrück, Barbarastr. 7, 49069 Osnabrück, Germany

Received 27 June 2006, revised 17 November 2006, accepted 13 December 2006
Published online 29 January 2007

PACS 77.84.Dy, 78.20.Ci, 78.30.–j

The index of refraction, the optical band edge and the Raman scattering of strontium barium niobate, $Sr_xBa_{1-x}Nb_2O_6$ with $0.38 < x < 0.77$ have been studied. The ordinary refractive index does not depend on x, while the extra-ordinary one increases with increasing x. The band edge is almost unaffected by the Ba- or Sr-content and shows a weak band bowing. Both the index of refraction and the band edge may be used for an optical determination of the composition of the crystal. Raman spectra show the typical behavior of tungsten bronze type crystals with broad bands and complicated spectral shapes.

1 Introduction

Recently the liquidus–solidus phase diagram of strontium barium niobate, $Sr_xBa_{1-x}Nb_2O_6$ has been determined over the whole existence region of the tetragonal phase [1]. This allows to tailor the well-known outstanding properties more precisely. Among these are photorefractive, electrooptic, nonlinear optic, and dielectric properties, with potential applications like pyroelectric detection [2], holographic data storage [3], phase conjugation [4], generation of photorefractive solitons [5], quasi-phase-matched second-harmonic generation [6], and electrooptic modulation [7].

The desirable improvements are governed by basic optical properties like the index of refraction and optical absorption near the bandedge. Since 1968 the index of refraction was known for three different compositions in a large wavelength range, see Venturini et al. [8], and served almost two decades as a reference, although the congruently melting composition had to be interpolated. This gave rise to obstacles for all device developments needing precise data. In 1987 Bhalla et al. [9] published index data of congruent SBN for two prominent laser lines (488; 632.8 nm) including the temperature dependence. For the visible the situation was improved for congruent SBN by Kip et al. [10, 11] first for a single line $\lambda = 514.5$ nm and then for $450 < \lambda < 650$ nm by introducing a Sellmeier equation derived from selected experimental data. Later the wavelength range was extended to unpoled and poled congruent SBN by Woike et al. [12] and an alternative Sellmeier equation was presented. This kind of Sellmeier equation is extended in this work by including the composition dependence which is based on experiments in a wide wavelength range.

In contrast to the index of refraction the bandedge was studied sofar in congruent material only. Polarized absorption spectra in a wide temperature range have been reported [13–16] and the lattice coupling has been interpreted by charge transfer vibronic exciton-states [14] or a one-oscillator model [16]. Both gave good fits, but the first suffers from parameter sets, which are not unique, preventing a physical interpretation.

* Corresponding author: e-mail: manfred.woehlecke@uos.de, Phone: +49 541 969 2631, Fax: +49 541 969 3512

2 Experimental details

For our investigations we used single crystals of SBN which were grown by the Czochralski technique using resistance heating; the growth procedure is described in detail by Ulex et al. [1]. Pyroelectric measurements [17] have shown that SBN is ferroelectric at room temperature throughout the whole composition range in which SBN crystals can be grown. Recent X-ray diffraction measurements [18] revealed that the ferroelectric phase is tetragonal with space group P4bm. Furthermore, it was shown that in the unfilled tungsten–bronze structure tetragonal sites (A1) are only occupied by Sr whereas pentagonal sites (A2) are shared by Sr and Ba. The site occupancy factor for Sr at the A1-sites is nearly constant while the site occupancy factors for Sr and Ba at the A2-sites vary with composition.

Extraordinary and ordinary refractive index measurements for as-grown SBN crystals covering the entire composition range for wavelengths from near infrared to the ultraviolet are reported. Eleven triangular prisms have been prepared with a composition varying from $x = 0.32$ to $x = 0.79$. Here the x-values refer to the crystal composition, determined by X-ray fluorescence [1], while Venturini et al. [8] have used the melt composition. The c-axis is aligned perpendicular to two parallel surfaces using a {100} growth face as reference. All sides were polished to optical quality. With the minimum deviation method the refractive indices were determined with an absolute accuracy better than ± 0.002 in the visible. The accuracy for the infrared is slightly worse due to the reduced detection sensitivity in this region. For the visible a mercury-lamp (seven emission lines) and for the infrared measurements two laser diodes of 790 and 1500 nm were used. All measurements were carried out at room temperature ($T = 22$ °C) and the light intensity was kept low to avoid sample heating.

Polarized absorption spectra were taken with a Bruins Instruments Omega 10 spectrometer with a wavelength accuracy of 0.1 nm, using mercury emission lines for calibration. Thin (0.5 mm) polished plates prepared from b- or c-cuts with various compositions were mounted in a gas flow cryostat with a temperature stability of about 2 K. Standard multiple pass reflection correction (see [19]) was done with a composition dependent index of refraction according to Eq. (1).

Raman scattering experiments have been performed in right-angle geometry using a Spex 14018 double monochromator and the 514.5 nm line of an argon ion laser with 1.2 W at room temperature. The spectral resolution was set to about 1 cm^{-1}. We measured SBN crystals $x = 0.38$ to 0.78. They were cut along the a-, b-, and c-axes, polished to optical quality and have a volume of about $4 \times 4 \times 6$ mm^3.

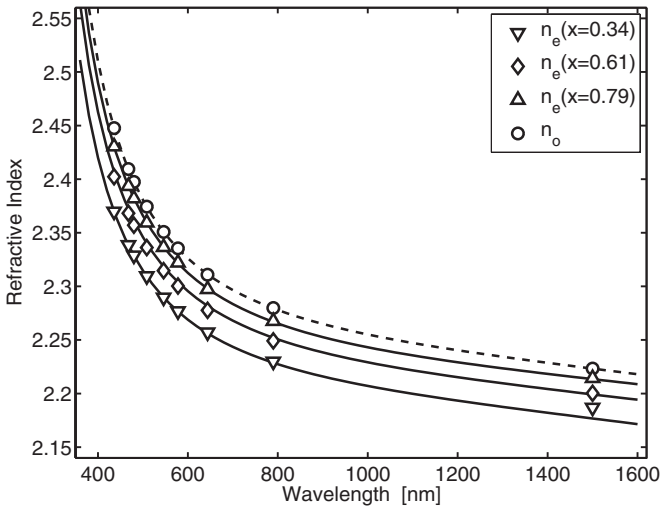

Fig. 1 Wavelength dependence of the index of refraction for three different compositions and the corresponding Sellmeier fits.

3 Results

3.1 Index of refraction

Figure 1 shows the measured n_o and n_e values for selected compositions together with the corresponding Sellmeier fits. The upper-most dashed line represents n_o for all compositions – within the measurement's accuracy the ordinary index of refraction does not noticeably depend on the composition. In contrast to this, the extraordinary index n_e exhibits a distinct monotonic increase with increasing strontium content x. A similar trend had been found by Venturini et al. [8] for three different melt compositions. To derive a global, composition dependent Sellmeier fit we used a conventional four-parameter equation and introduced modified parameters which linearly depend on the Sr-content x:

$$n^2(x,\lambda) = A_0 + A_1 x + \frac{B_0 + B_1 x}{\lambda^2 - C_0 - C_1 x} - (D_0 + D_1 x)\,\lambda^2 \,. \tag{1}$$

The corresponding parameters for n_o and n_e are listed in Table 1.

Usually the composition dependence of refractive indices can be explained by a corresponding frequency shift of the dominating oscillator in the ultraviolet region, expressed in the Sellmeier parameter C. Such a frequency shift, however, should affect *all* refractive indices and, furthermore, should also show up in a shift of the absorption edge (see following chapter).

A critical examination of the Sellmeier parameters in Table 1 reveals that the main contribution to the composition dependence of the extraordinary index is constant, imposed by parameter A_1. Such a constant contribution can be introduced by the static polarization of the material via the quadratic electrooptic effect. According to Ref. [9], for SBN this electrooptic contribution, Δn_i, to the refractive indices can be written as

$$\Delta n_o = -g_{13}(n_o^0)^3 P_3^2/2 \,, \tag{2}$$

$$\Delta n_e = -g_{33}(n_e^0)^3 P_3^2/2 \,, \tag{3}$$

where g_{ik} are the components of the electrooptic tensor in contracted notation, n_i^0 are the refractive indices for the unpolarized material, and P_3 is the static polarization of the material. The data presented in Ref. [9] show that $g_{13} \ll g_{33}$, thus only the extraordinary index is affected. For g_{33} a value of approximately 0.10 m^4/C^2 at 633 nm is given.

Pyroelectric measurements on SBN [17] yielded values for the polarization at room temperature spanning from 0.28 C/m^2 for $x = 0.34$ to 0.11 C/m^2 for $x = 0.79$. Using Eq. (3), corresponding Δn_e values of $\Delta n_e(0.34) = -0.0477$ and $\Delta n_e(0.79) = -0.0061$ can be calculated, yielding a difference of $\delta n_e^{eo} = -0.0416$ between these two compositions due to the electrooptic contribution. From the Sellmeier equation, on the other hand, the extraordinary refractive indices at 633 nm for the two compositions are $n_e(0.34, 633) = 2.2589$ and $n_e(0.79, 633) = 2.3015$, respectively, yielding a difference of $\delta n_e^{exp} = -0.0426$.

Table 1 Parameters for the Sellmeier equations for n_o and n_e as a function of composition.

	n_o	n_e
A_0	5.002	4.712
A_1	0	0.291
B_0 (nm^2)	1.272×10^5	9.242×10^4
B_1 (nm^2)	0	4.398×10^4
C_0 (nm^2)	6.261×10^4	5.679×10^4
C_1 (nm^2)	0	3.62×10^3
D_0 (nm^{-2})	5.207×10^{-8}	6.21×10^{-8}
D_1 (nm^{-2})	0	-2.27×10^{-8}

This means that the experimentally found composition dependence of the extraordinary index can be fully attributed to the electrooptic contribution varying according to the composition dependent static polarization.

3.2 Absorption edge

Often a band edge property like the energy dependence of a fixed absorption value $\alpha_{const}(E)$ can serve as nondestructive method to determine the crystal composition. But a necessary prerequisite for such an application is a monotonic dependence of $\alpha_{const}(E)$. Unfortunately this is not fulfilled in $Sr_xBa_{1-x}Nb_2O_6$, where we found a band bowing, as can be seen in Fig. 2, where $\alpha_{100}(E)$ was used to define the bandedge. At such a high absorption we can expect direct transitions [20]. The observed energy change between the congruent composition and the limits above and below is about 15 meV corresponding to about 1.5 nm. Thus careful absorption measurements may serve as a tool to determine the crystal composition more precisely, provided that one knows whether the true composition is above or below the congruently melting one.

Because the band edge does not follow Vegards rule, a description according to

$$E_g(x) = E_g^A(1-x) + E_g^B x - bx(1-x) \tag{4}$$

is often introduced, where (E_g^A; E_g^B) are the band gap energies of the subsystems and b, characterizing the deviation from linearity, is called the bowing parameter. Several band structure models have been proposed to predict the value of b. Most of these models describe b adequately but differ particularly in how the effect of disorder of different cations (anions) is treated in the band structure [21]. Theoretical studies have been hampered by the problems of incorporating inhomogeneities into periodic crystals. The virtual-crystal approximation is one approach to overcome these difficulties. Using this method a composite potential is constructed which represents the average of the component atoms comprising the inhomogeneity. Already in 1983 A. Zunger and J. E. Jaffe [22] pointed out that often the anion-cation bond lengths do not average to a single bond but instead remain close, throughout the composition range, to their respective values in the endpoints. To gain more insight into the physics Bernard and Zunger [23] proposed a decomposition of the bowing parameter into physically distinct contributions like the volume deformation, the charge exchange and the structural relaxation. We are not aware of any calculation of

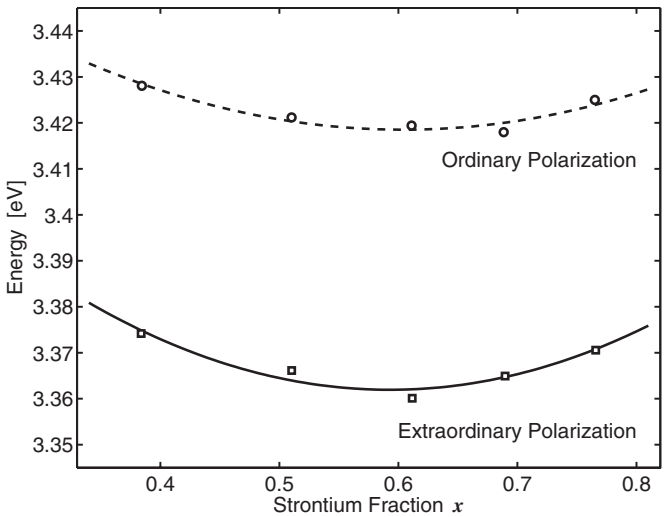

Fig. 2 Band edge of $Sr_xBa_{1-x}Nb_2O_6$ for the polarized absorption for absorption values $\alpha_{100}(E)$ at room temperature.

Table 2 Fit parameter for the composition dependence of the band edge energy.

	E_g^A (eV)	E_g^B (eV)	b (eV)
o. pol. light	3.494	3.451	0.207
e. pol. light	3.466	3.411	0.296

the bowing parameter in SBN, therefore we present the parameters (Table 2) but are unable to perform a conclusive decomposition.

Although the band edge energy $E_g(x)$ varies with x, the weak bending for both ordinary and extra-ordinary light polarization cannot cause the different behavior of the index of refraction. But it is tempting to correlate the weakness of the bending with structural changes. According to the classical work of DiDomenico and Wemple [24] the optical properties of compounds with NbO_6 octahedra are governed by these units. Extensive structure studies [25] revealed that the Nb–O interatomic distance is independent of x for one of the two different oxygen-octahedra, but depends on x for the other one. In this octahedron the Nb–O distance increases with larger x-values for one apex ion, while it decreases for the other. Such a reverse trend may cause some bend bowing, but we point out that this simple idea cannot explain the exact shape or the size of the bending. The different Nb–O distances in c-direction of the crystal and perpendicular to it [18] explain the difference between the absorption edge for ordinary and that for extraordinary polarisation. For unique distances the absorption edges would be equal. A shift of the Nb-ion in c-direction causes a decrease of the extraordinary dipole transition energy for one Nb–O in c-direction, an increase for the opposite one. The decreased will govern the absorption edge. In contrast to this, the ordinary dipole transition energy will remain practically unchanged.

In Fig. 3 we plotted the temperature dependence of $E(\alpha_{100}, T)$ for SBN with $x = 0.689$ for both light polarizations. For all the other compositions the temperature dependence of the band edge has the same behavior. For a temperature higher than $T = 200$ K there exists a linear dependence which turns into a flat part for T below 100 K. We did not notice any peculiarities of the absorption in the phase transition region. The band edge temperature expression $E_g(T)$ have the general form $E_g^0 - KN$, where K describes the electron–lattice coupling and N the phonon occupation number. Expressions for the occupation number N are usually based on the Bose–Einstein statistics. For describing the temperature dependence of the band edge it is sufficient to use a single Einstein oscillator because the internal energy of a set of optical

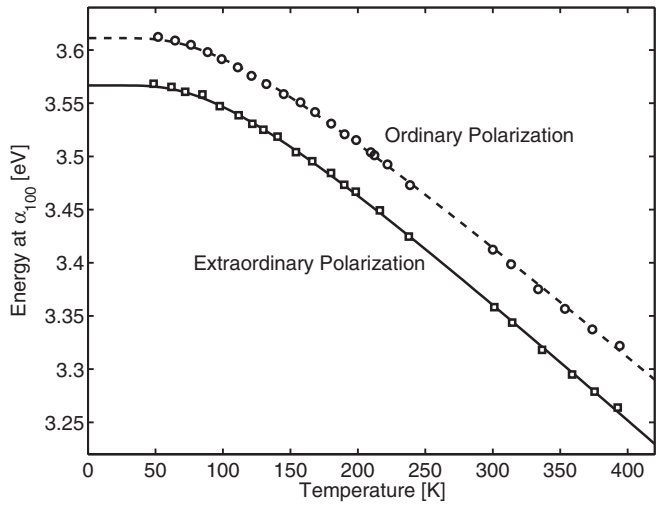

Fig. 3 Temperature dependence of the band edge in SBN taken at an absorption value of $\alpha = 100$ cm^{-1} for ordinary and extra-ordinary light polarization.

phonon modes having different energies is very closely equal to the internal energy of a single phonon system with an energy being the average of the multi-phonon set [26]. For fitting the data we adopted the expression in [16],

$$E_g(T) = E_g(0) - \beta k\Theta\left(\frac{1}{\exp(\Theta/T)-1}\right). \tag{5}$$

$E_g(0)$ is the energy at $T = 0$, β is a dimensionless coupling constant describing the slope of E_g for high temperatures ($T \to \infty$), while $k\Theta$ is the phonon energy. Specific parameters are the composition independent values $\beta_{o,e} = 12.4, 13.1$ for *o*. and *e*. polarisation, respectively, as well as $\Theta_{o,e} = 290, 270$ K and a composition dependent value for E_g^0 calculated with Eq. (4) and adding 0.01 eV.

With these averaged values we obtained a slope $\beta k = -1.1$ meV/K which is in agreement with a value of -1.2 meV/K for $x = 0.5$ derived from direct transitions [27].

3.3 Raman Scattering

The outstanding properties and the potential applications of SBN have pushed many informative studies, but no detailed report on the compositional dependence of the vibrational properties have been published. This is mainly due to missing crystals and the complex unfilled tungsten–bronze structure with the tetragonal space group P4bm and the point group 4mm having five formula units per unit cell. This results in 135 vibrational modes including three acoustic ones. These modes are characterized by the irreducible representations A_1, A_2, B_1, B_2 and E, all except A_2 being Raman active [28]. Two mode frequencies have been mentioned in a work by Burns et al. [29] devoted to other tungsten-bronze compounds. A first detailed investigation of polarized Raman scattering including an assignment was reported in 1971 [28] for two compositions, i.e. $x = 0.5$ and $x = 0.75$. Based on scattering diagrams and distinguishing between longitudinal and transverse modes, more or less pronounced frequency shifts for all symmetry species of the two compositions were reported. A first temperature study was performed in 1973 [30]. Later some frequencies below 100 cm^{-1} were added in a study of the temperature dependence of the modes in $Sr_{0.75}Ba_{0.25}Nb_2O_6$ [31]. Raman spectra of a congruently melting sample were published for the first time in 1990 by Burns and co-workers, but no new modes were introduced [32]. More detailed information for a congruent sample was presented one year later by Wilde [33]. No Raman spectra are known for crystals with melt compositions $x < 0.5$ and due to a possible crosstalk of strong A_1 modes governed by diagonal Raman tensor elements the assignment of some weak modes should be checked. Therefore we measured room-temperature Raman spectra of A_1, B_1, B_2 and E modes for various scattering configurations and compositions.

In Fig. 4 spectra for ten different compositions in the $x(zz)y$ configuration corresponding to transversal A_1 modes, denoted TA_1, are shown. Two strong and broad lines are accompanied by several weak ones. Apart from two weak modes at about 125 and 155 cm^{-1} all other ones strongly increase in intensity with reduced Sr-content. For the two dominant modes (256, 630 cm^{-1}) this is associated with a shape change of the low energy wing. Because of background problems we have deconvoluted only the last one and found two components decreasing linearly in frequency in almost the same manner with the Sr-content ($x = 0.4 \ldots 0.76$: 643 . . . 632 cm^{-1}; 602 . . . 586 cm^{-1}). This mode is believed to be of a stretch type vibration of the NbO_6 octahedron. There are two crystallographically independent octahedra, $Nb(1)O_6$ surrounded by two triangular and two pentagonal channels, the first being empty. The second type, $Nb(2)O_6$, is surrounded by a triangular, a tetragonal and two pentagonal channels [25]. Both octahedra have a site multiplicity ratio of 4, which is in reasonable agreement with the experimental ratio of 3.3 for the intensity of the components. Thus we ascribe the low energy mode to the $Nb(1)O_6$ octahedra. The decrease of the frequencies with increasing Sr-content correlates roughly with the decrease of the acentric distortions of the corresponding octahedra. A composition dependent change of the anisotropy of electrostatic forces can be ruled out, because only TA_1 modes are involved.

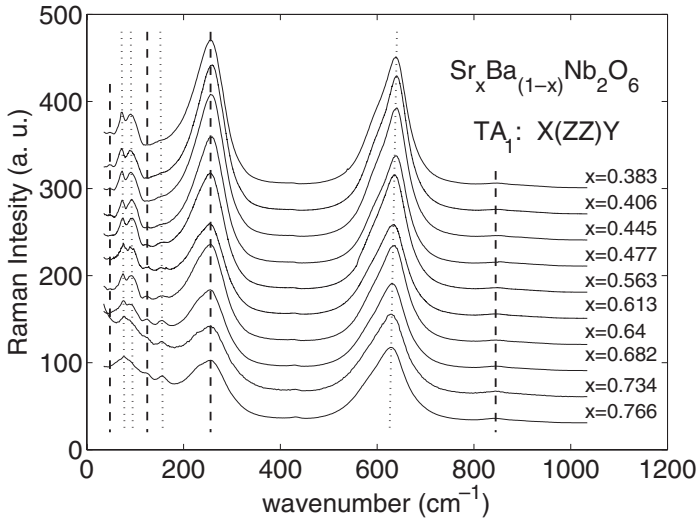

Fig. 4 Composition dependence of the TA_1 mode at room temperatur. The dashed lines are guides for the eye and indicate modes which do not depend on composition (shift less than 2 cm^{-1}). The dotted lines point to composition-dependent modes.

For energies less than 200 cm^{-1} we observed four well resolved modes, for more details see Table 3. Almost all lines have been already mentioned [31–33], but often as a shoulder in a spectrum for only one composition. The frequencies agree within experimental error of about 2 cm^{-1} with those of Wilde [33], but deviate stronger from [31], which is probably due to different crystal qualities. The decrease of the intensity of the modes at 155 and 125 cm^{-1} with decreasing Sr-content clearly points to an

Table 3 Energies (given in cm^{-1}) for A_1, E, B_2, and B_1 modes at room temperature for $x = 0.383$ and $x = 0.766$; w = weak, d = from deconvolution, s = shoulder, and b = broad.

TA_1 $x(zz)y$		LE, TE $x(yz)y$		B_2 $x(yx)y$		QL, QT and B_1 $x(yy)z$	
0.383	0.766	0.383	0.766	0.383	0.766	0.383	0.766
844 (w)	844 (w)					848	848
644 (d)	633 (d)	648 (b)	631	~ 630 (s)	~ 630 (s)	629 (d)	629 (d)
602 (d)	587 (d)					590 (d)	579 (d)
		544	550	550	550		
				490	493	515 (d)	515 (d)
				415	415		
		310 (s)	316 (s)	294			
256	256	257	257				
				194	191	187	187
153	156	167	178			141	141
125	125						
94	92	98	98 (s)	97	101	103	103
73	77	77	79	80	81		
47	47			52	56		58
						38	32

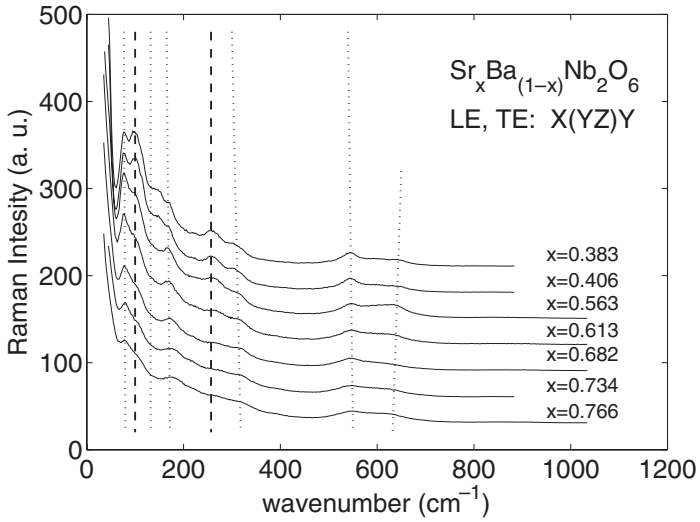

Fig. 5 Composition dependence of the *E* mode at room temperature. The dashed lines are guides for the eye and indicate modes which do not depend on the composition (shift less than 2 cm^{-1}). The dotted lines point to modes depending on the composition.

external vibration governed by Sr. The opposite holds for the mode at about 90 cm^{-1}, where an increase of Ba is involved in a growing feature. The almost stable mode at 77 cm^{-1} may be due to the constant occupation factor of Sr–A1 sites [18]. We continue with the weak feature at 47 cm^{-1}. This grows with increasing Ba-content and was first observed by Burns et al. [32] in $z(yz)x$ configuration as an *E* mode but not in $x(zz)y$ as an A_1 mode, while in the present study the mode is not observed in the $z(yz)x$ configuration, see Fig. 5. The fact that the mode is missing in the A_1-spectrum of Burns et al. [32] and in the *E*-spectrum in Fig. 5 is easily explained by the strong Rayleigh wings in both cases. Because this mode

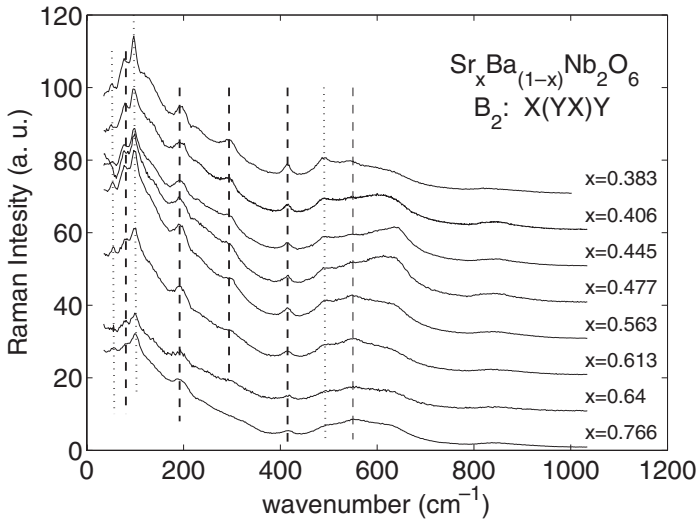

Fig. 6 Composition dependence of the B_2 mode at room temperature. The dashed lines are guides for the eye and indicate modes which do not depend on the composition (shift less than 2 cm^{-1}). The dotted lines point to modes depending on the composition.

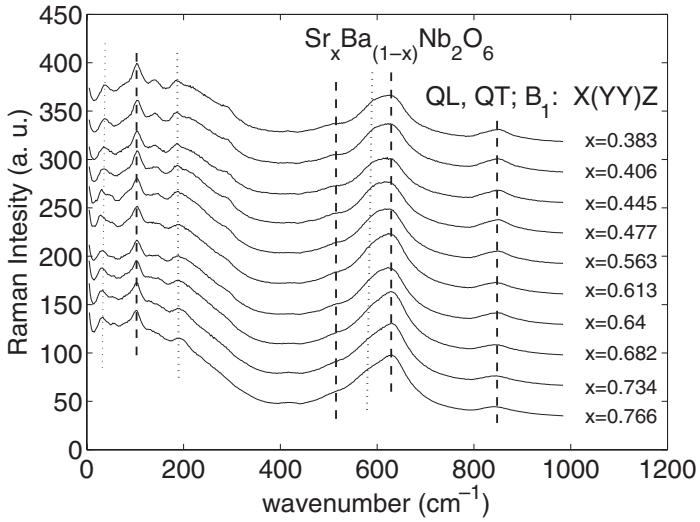

Fig. 7 Composition dependence of the B_1 mode at room temperature. The dashed lines are guides for the eye and indicate modes which do not depend on the composition (shift less than 2 cm^{-1}). The dotted lines point to modes depending on the composition.

is more or less well resolved for all compositions below the congruent one, we have strong evidence for an A_1-mode, but cannot exclude a crosstalk combined with a line broadening for compositions above the congruent one. Finally we mention the very weak and almost composition independent feature at 844 cm^{-1}. Such a mode shows up in several tungsten bronze type crystals with NbO_6 building units and is believed to belong to a stretch type vibration [34].

In Fig. 5 modes are shown which mainly increase with growing Ba-content, some change in addition their frequencies, others stay stable. None mode is dominant like for A_1 species, a behavior usually observed in tungsten bronze type crystals. Again the observed frequencies for a congruent composition coincide with those reported in [33], except that a very low energy mode is missing in our spectra, because of a strong Rayleigh wing. The shape of the spectra between 500 and 700 cm^{-1} may hide more modes, but the possibility of a crosstalk of the strong A_1 modes in this spectral range makes a conclusive deconvolution almost impossible. Unfortunately the situation is only slightly better for the B_2-spectrum, see Fig. 6. There is some evidence for at least four modes in the region between 400 and 700 cm^{-1}. The mode at 490 cm^{-1} mentioned in [33] as a shoulder, is at least clearly resolved for Ba-rich SBN.

Finally we discuss the $x(yy)z$ scattering configuration with B_1-modes and QL and QT A_1 modes. Besides the bands at about 848 and 630 cm^{-1} no clear coincidence with A_1-mode spectra (Fig. 4) is observed, in agreement with the results of Wilde [33] for congruent material. A deconvolution of the structures between 450 and 700 cm^{-1} revealed a linear shift of only one mode with composition, the other two are stable in energy, with weak changes of the intensity of the components, see Table 3 and Fig. 7. Almost all bands showing up below 200 cm^{-1} have already been reported [28, 33], except the composition dependence of the low energy one. In general the influence of the crystal composition on $x(yy)z$ spectra is weak.

To sum up, one can say that $Sr_xBa_{1-x}Nb_2O_6$ follows the general trends of Raman spectra in tungsten bronze type crystals, i. e. two strong A_1 modes at 250 and 630 cm^{-1}, broad bands consisting of several LO and TO modes. A composition dependent deconvolution recealed additional modes, sofar only indicated as shoulders. The variation of the Sr/Ba ratio is reflected in the spectra, but a complete unambiguous assignment is still a problem.

4 Conclusion

Optical (index of refraction n, bandedge-absorption E_g) and vibrational (Raman scattering) properties of strontium barium niobate samples, $Sr_xBa_{1-x}Nb_2O_6$, with $0.38 < x < 0.77$ have been comprehensively studied. The extraordinary refractive index and the Raman spectra show a pronounced dependence on the composition, while the bandedge position is almost insensitive and the ordinary index even constant. Because of this different behavior of the related quantities n, E_g, the usual interpretaion with a frequency shift of the dominating oscillator in the ultraviolet region fails. From the composition dependent parameters of the Sellmeier equation for n we concluded that the composition dependence of the extraordinary index can be fully attributed to the electrooptic contribution varying according to the composition dependent static polarization. The weak bend bowing is tentatively attributed to opposite changes of the Nb–O distances in the two structurally different NbO_6 octahedra. Raman scattering results in four scattering configurations revealed new insight in the number of modes and their compositional dependence, particularly due to a better spectral resolution for some compositions and deconvolutions based on several compositions. A mode splitting of A_1 modes was attributed to different vibrations of the two distinct NbO_6 octahedra.

References

[1] M. Ulex, R. Pankrath, and K. Betzler, J. Cryst. Growth **271**, 128 (2004).
[2] A. M. Glass, J. Appl. Phys. **40**, 4699 (1969).
[3] F. Kahmann, J. Höhne, R. Pankrath, and R. A. Rupp, Phys. Rev. B **50**, 2474 (1994).
[4] H. Y. Zhang, X. H. He, Y. H. Shih, and L. Yan, J. Mod. Opt. **41**, 669–674 (1994).
[5] M. Wesner, C. Herden, R. Pankrath, D. Kip, and P. Moretti, Phys. Rev. E **64**, 036613 (2001).
[6] A. S. Kewitsch, M. Segev, A. Yariv, G. J. Salamo, T. W. Towe, E. J. Sharp, and R. R. Neurgaonkar, Appl. Phys. Lett. **64**, 3068–3070 (1994).
[7] R. R. Neurgaonkar, W. K. Cory, J. R. Oliver, E. J. Sharp, M. J. Miller, G. L. Wood, W. W. Clark III, A. G. Mott, G. J. Salamo, and B. D. Monson, Proc. SPIE **1148**, 2 (1989).
[8] F. L. Venturini, E. G. Spencer, P. V. Lenzo, and A. A. Ballman, J. Appl. Phys. **39**, 343 (1968).
[9] A. S. Bhalla, R. Guo, L. E. Cross, G. Burns, F. H. Dacol, and R. R. Neurgaonkar, Phys. Rev. B **36**, 2030 (1987).
[10] D. Kip, S. Aulkemeyer, and P. Moretti, Opt. Lett. **20**, 1256–1258 (1995).
[11] D. Kip, S. Aulkemeyer, K. Buse, F. Mersch, R. Pankrath, and E. Krätzig, phys. stat. sol. (a) **154**, K5–K7 (1996).
[12] T. Woike, T. Granzow, U. Dörfler, C. Poetsch, M. Wöhlecke, and R. Pankrath, phys. stat. sol. (a) **186**, R13–R15 (2001).
[13] J. Seglins and S. Kapphan, phys. stat. sol. (b) **188**, K43–K45 (1995).
[14] V. S. Vikhnin, S. Kapphan, and J. Seglins, J. Korean Phys. Soc. **32**, S621–S623 (1998).
[15] V. S. Vikhnin, S. Kapphan, and J. Seglins, Radiat. Eff. Defects Solids **150**, 109–114 (1999).
[16] M. Meyer, M. Wöhlecke, and O. F. Schirmer, phys. stat. sol. (b) **221**, R1–R3 (2000).
[17] C. David, T. Granzow, A. Tunyagi, M. Wöhlecke, Th. Woike, K. Betzler, M. Ulex, M. Imlau, and R. Pankrath, phys. stat. sol. (a) **201**, R49–R52 (2004).
[18] S. Podlozhenov, H. Graetsch, J. Schneider, M. Ulex, M. Wöhlecke, and K. Betzler, Acta Crystallogr. B **62**, 960–965 (2006).
[19] L. Kovács, G. Ruschhaupt, K. Polgár, G. Corradi, and M. Wöhlecke, Appl. Phys. Lett. **70**, 2801–2803 (1997).
[20] V. V. Voronov, Yu. S. Kuzminov, and I. G. Lukina, Sov. Phys. Solid State **18**, 598–600 (1976).
[21] J. A. Van Vechten and T. K. Bergstresser, Phys. Rev. B **1**, 3351 (1970).
[22] A. Zunger and J. E. Jaffe, Phys. Rev. Lett. **51**, 662 (1983).
[23] J. E. Bernard and A. Zunger, Phys. Rev. B **36**, 3199 (1987).
[24] M. DiDomenico and S. H. Wemple, J. Appl. Phys. **40**, 720 (1969).
[25] T. S. Chernaya, B. A. Maksimov, T. R. Volk, L. I. Ivleva, and V. I. Simonov, Phys. Solid State **42**, 1716–1721 (2000).
[26] D. Redfield and W. J. Burke, J. Appl. Phys. **45**, 4566 (1974).
[27] V. G. Savitskii, R. N. Kovtun, V. E. Aleksyuk, and P. F. Protsakh, Sov. Phys. Solid State **15**, 2464 (1974).

[28] E. Amzallag, T. S. Chang, R. H. Pantel, and R. S. Feigelson, J. Appl. Phys. **42**, 3254 (1971).
[29] G. Burns, J. D. Axe, and D. F. O'Kane, Solid State Commun. **7**, 933–936 (1969).
[30] K. G. Bartlett and L. S. Wall, J. Appl. Phys. **44**, 5192–5193 (1973).
[31] Kh. Sh. Rustamov, V. S. Gorelik, Yu. S. Kuz'minov, G. V. Peregudov, and M. M. Sushchinskii, Sov. Phys. Solid State **18**, 1988–1990 (1976).
[32] G. Burns, F. H. Dacol, R. R. Neurgaonkar, A. S. Bhalla, and R. Guo, Ferroelectrics **108**, 189–193 (1990).
[33] R. E. Wilde, J. Raman Spectrosc. **22**, 321–325 (1991).
[34] H. R. Xia, H. Yu, H. Yang, K. X. Wang, B. Y. Zhao, J. Q. Wei, J. Y. Wang, and Y. G. Liu, Phys. Rev. B **55**, 14892–14898 (1997).